# Complete set of precise deuteron analyzing powers at intermediate energies: Comparison with modern nuclear force predictions

K. Sekiguchi,[1,*] H. Sakai,[1,2] H. Witała,[1,3] W. Glöckle,[4] J. Golak,[3,4] M. Hatano,[1] H. Kamada,[4] H. Kato,[1] Y. Maeda,[1] J. Nishikawa,[5] A. Nogga,[4] T. Ohnishi,[2] H. Okamura,[5] N. Sakamoto,[2] S. Sakoda,[1] Y. Satou,[2] K. Suda,[5] A. Tamii,[1] T. Uesaka,[5] T. Wakasa,[6] and K. Yako[1]

[1]*Department of Physics, University of Tokyo, Bunkyo, Tokyo 113-0033, Japan*
[2]*The Institute of Physical and Chemical Research (RIKEN), Wako, Saitama 351-0198, Japan*
[3]*Institute of Physics, Jagiellonian University, PL-30059 Cracow, Poland*
[4]*Institut für Theoretische Physik II, Ruhr-Universität Bochum, D-44780 Bochum, Germany*
[5]*Department of Physics, Saitama University, Saitama 338-8570, Japan*
[6]*Research Center for Nuclear Physics, Osaka University, Ibaraki, Osaka 567-0047, Japan*

(Received 10 September 2001; published 12 February 2002)

Precise measurements of deuteron vector and tensor analyzing powers $A_y^d$, $A_{xx}$, $A_{yy}$, and $A_{xz}$ in $d$-$p$ elastic scattering were performed via $^1\mathrm{H}(\vec{d},d)p$ and $^1\mathrm{H}(\vec{d},p)d$ reactions at three incoming deuteron energies of $E_d^{\mathrm{lab}}=140$, 200, and 270 MeV. A wide range of center-of-mass angles from $\approx 10°$ to 180° was covered. The cross section was measured at 140 and 270 MeV at the same angles. These high precision data were compared with theoretical predictions based on exact solutions of three-nucleon Faddeev equations and modern nucleon-nucleon potentials combined with three-nucleon forces. Three-body interactions representing a wide range of present day models have been used: the Tucson-Melbourne $2\pi$-exchange model, a modification thereof closer to chiral symmetry, the Urbana IX model, and a phenomenological spin-orbit ansatz. Large three-nucleon force effects are predicted, especially at the two higher energies. However, only some of them, predominantly $d\sigma/d\Omega$ and $A_y^d$, are supported by the present data. For tensor analyzing powers the predicted effects are in drastic conflict to the data, indicating defects of the present day three-nucleon force models.

DOI: 10.1103/PhysRevC.65.034003 PACS number(s): 21.30.−x, 21.45.+v, 24.10.−i, 24.70.+s

## I. INTRODUCTION

One current interest for the investigations of few-nucleon system focuses on the study of three-nucleon force (3NF) properties in the three-nucleon continuum. One of the main goals of experimental and theoretical pursuits is to establish the relevance of the 3NF in the nuclear Hamiltonian, in terms of which nuclear phenomena can be understood. Despite the fact that the meson-exchange picture undoubtedly predicts such forces, 3NFs cause only a small perturbation to mostly pairwise interactions of three nucleons. Their clear signature can only be seen in precise experimental data. Therefore, to find evidence for them and to nail down their properties present a hard task.

Decades of intensive theoretical and experimental efforts led recently to a new generation of realistic nucleon-nucleon ($NN$) potentials: AV18 [1], CD-Bonn [2–4], Nijm I, II, and 93 [5]. They have been constructed using meson-exchange or more phenomenological approaches with the aim to describe the rich set of experimental $NN$ data as precisely as possible. This nontrivial aim has been achieved with unprecedented precision of a $\chi^2$ per data point very close to one. Those realistic $NN$ forces fail to provide experimental binding energies of few-nucleon systems and lead to clear underbinding. For three- and four-nucleon systems, where exact solutions of the Schrödinger equation are available, this underbinding amounts to 0.5–1 MeV in the case of $^3$H and $^3$He, and to 2–4 MeV for $^4$He [6]. For systems with more nucleons, where stochastic techniques [7,8] allow us to go up to $A=8$ nuclei, the underbinding is as large as $\approx 10$ MeV. Natural candidates to fill the gaps are 3NFs. The most representative and early version of a 3NF model is the Fujita-Miyazawa force [9], a $2\pi$ exchange between three nucleons with an intermediate $\Delta$ excitation. Later this mechanism has been incorporated into more refined theoretical 3NF models, such as the Tucson-Melbourne (TM) 3NF [10,11] and the Urbana IX three-body interaction [12]. For $3N$ and $4N$ systems, one can achieve the correct binding energies with the TM or Urbana IX 3NFs. However, in case of higher-mass nuclei up to $A=8$ only a reduction of the underbinding for the low-energy bound states follows, leaving in addition an insufficient spin-orbit splitting of some nuclear levels [7,13]. Thus those first promising signals for 3NF effects also indicate simultaneously deficiencies of present day 3NF models. Comparison of theoretical and experimental binding energies points to the necessity of a 3NF and is used mainly to constrain its overall strength. A more detailed investigation of 3NF properties offers the $3N$ continuum, where a rich set of spin observables is available in elastic nucleon-deuteron ($Nd$) scattering and the deuteron breakup processes.

The recent progress in computational resources made it possible to perform rigorous numerical Faddeev-type calculations for the $3N$ scattering processes using $2N$ and $3N$ forces [14–16]. It provided the possibility to use $3N$ scattering processes with their rich set of spin observables as a unique tool for a more detailed investigation of 3NF properties than offered by bound states. This together with an ex-

*Email address: kimiko@nucl.phys.s.u-tokyo.ac.jp

 

perimental access to high precision data for the cross sections and spin observables in $Nd$ elastic scattering and the breakup processes will form a solid basis to test the $3N$ Hamiltonian. Especially interesting are spin observables at higher energies ($E/A \gtrsim 20$ MeV) with the initial nucleon and/or deuteron polarized and where the polarization of the outgoing particles is also measured. This was proposed in Ref. [17]. Even the simplest observables, the unpolarized cross section and first-order spin observables, such as the vector and tensor analyzing powers, are of great importance. At lower energies ($E/A \lesssim 20$ MeV), theoretically predicted 3NF effects are rather small, and indeed a generally good description of $Nd$ elastic scattering data by $2N$ forces only is obtained [16,18]. The only clear-cut exceptions are the low energy vector analyzing powers, for which drastic discrepancies exist between all realistic $2N$ force predictions and the data in the region around the maximum near $\theta_{\mathrm{c.m.}} = 120°$ [16,19]. This was first pointed out by Koike and Haidenbauer [20]. These discrepancies are seen in the neutron-deuteron ($nd$) and proton-deuteron ($pd$) data for the cases of polarized nucleons ($A_y$) and polarized deuterons ($A_y^d$). One possible reason for these discrepancies might lie in the insufficient knowledge of the ${}^3P_j$ $NN$ force components [21] to which the low energy vector analyzing powers are very sensitive. There is also good reason to expect that 3NFs beyond the ones already mentioned might cure these discrepancies. This is suggested by chiral perturbation theory [22,23]. The predicted effects of the present day 3NF models for these observables are very small [17,18].

The first evidence for strong 3NF effects in the $3N$ continuum came from a study of the minima of the $Nd$ elastic scattering cross sections at incoming nucleon energies greater than $\approx 60$ MeV [24]. A large part of the discrepancy between the data and predictions based exclusively on $NN$ forces could be removed, when the $2\pi$-exchange TM 3NF properly adjusted to the triton binding energy was included in the 3N Hamiltonian. A coupled channel study of $Nd$ scattering including $\Delta$-isobar excitation [25] leads to similar improvements. Also a precise measurement of the $nd$ total cross section [26,27] revealed that a discrepancy between the data and the $2N$ force predictions at energies above $\approx 100$ MeV is mostly removed by the TM 3NF. In this case, however, the data possibly also indicate a growing importance of relativistic effects with increasing energy [27].

One can expect that also polarization observables at higher energies, similar to the cross section, will exhibit 3NF effects. However, the existing higher-energy data basis for proton analyzing powers is rather poor. To the best of our knowledge up until recently there were only seven data sets, six from $pd$ (65 MeV [28], 120 MeV [29], 135 MeV [30], 146 MeV [31], 155 MeV [32], 200 MeV [29,33]) and one from $nd$ (65 MeV [34]) measurements. With the exception of the precise polarization measurements of Refs. [28] and [33] the other sets exhibit large uncertainties in the interesting angular range or cover it only partially. Very recently the situation for this observable significantly improved with the new data of Refs. [35–38]. For the deuteron analyzing powers, the situation is more unsatisfactory. The only existing measurements of deuteron vector and tensor analyzing powers are those of Ref. [39] covering the incoming nucleon energies from 32 MeV to 93.5 MeV, with only five data sets above 60 MeV (66.5, 72, 78, 86 m and 93.5 MeV). However, these data are of restricted value to draw conclusions about 3NF effects due to the large uncertainty in the incoming deuteron energy ($\Delta E_d^{\mathrm{lab}} \approx 5-6$ MeV), large error bars, and/or the limited angular range covered by those measurements. The old data for $T_{20}$ at a number of energies were taken only at $\theta_{\mathrm{c.m.}} = 180°$ [40]. Recently $pd$ data at 197 MeV for $A_y^d$ have been taken [37] covering, however, only a restricted angular range. The older data taken at deuteron beam energies of 191 and 395 MeV [41] have large error bars.

The developments in technology of highly polarized proton and deuteron ion sources as well as their application in recently constructed accelerators, together with new sophisticated techniques of target polarization, made it now possible to get much more precise data for the spin observables, not only in the low-energy region ($E/A \lesssim 20$ MeV), but also at the higher energies ($E/A \gtrsim 20$ MeV). The constructions of high precision polarimeters also allowed us recently to get accurate data on more complex spin polarization transfer observables [42].

In the framework of our polarized deuteron beam project, a polarized deuteron ion source [43] was constructed at RIKEN together with the development of a spin rotation Wien filter system [44], allowing one to direct the spin in any direction, which is especially important for applying it with the RIKEN SMART (a swinger and a magnetic analyzer with rotators and twisters) magnetic spectrograph [45]. A calibration of the higher energy in-beam deuteron polarimeter was achieved in our previous measurement of $d$-$p$ elastic scattering at $E_d^{\mathrm{lab}} = 270$ MeV, which covered the angular range of $\theta_{\mathrm{c.m.}} = 60° - 140°$ [46].

In view of the success in obtaining high precision spin observables in our earlier experiments [47–49], the experimental setup has been modified to extend the measurement to all deuteron analyzing powers ($A_y^d$, $A_{yy}$, $A_{xx}$, and $A_{xz}$) together with the cross section for $d$-$p$ elastic scattering at $E_d^{\mathrm{lab}} = 270$ MeV to a much wider angular range of $\theta_{\mathrm{c.m.}} = 10° - 180°$ [42]. In Ref. [42] the data were compared with the theoretical predictions based on various $NN$ potentials combined with the TM 3NF. The discrepancy in the cross section minimum to $NN$ force predictions only is removed by adding the TM 3NF, as is predicted in Ref. [24]. The inclusion of the TM 3NF removes even the discrepancy at backward angles. For the deuteron analyzing power $A_y^d$ the TM 3NF is similarly successful as in the case of the cross section in filling the gap between the data and the pure 2N force predictions. Note that the recent data for $A_y^d$ and the spin correlation coefficient $C_{y,y}$ at 197 MeV by Cadman *et al.* [37] are also reproduced by adding the TM 3NF. However, for the deuteron tensor analyzing powers the theoretically predicted TM 3NF effects do not improve the description of the experimental data, and this presents a great challenge to theoreticians. Recently, nucleon vector analyzing power data have revealed the deficiency of this particular

3NF model [35–38], which produces large but wrong effects. In this case the Urbana IX and TM′ 3NFs (the TM′ is a version of the TM 3NF that is more consistent with chiral symmetry [22,23,50]) are much more successful and lead to rather good agreement with the data [17,38].

In Ref. [17] it was documented that the most popular current 3NF models show large effects for many spin observables in elastic $Nd$ scattering. Clearly the present situation is only the very beginning for the investigation of the spin structure of the 3NF. More numerous high precision data are needed to provide constraints on theoretical 3NF models. It is the aim of the present study to provide a complete set of high precision data for deuteron analyzing powers at incoming deuteron energies $E_d^{\rm lab}=140$, 200, and 270 MeV, and to compare them with present day 3NF predictions. Some of the data at 270 MeV have been reported previously [42]. In addition to the extension of the measurement to other energies we cover now a wider angular range up to the very backward region of angles $\theta_{\rm c.m.}=10°-180°$.

In Sec. II we present the details of the experimental arrangement and Sec. III deals with the data analysis and the experimental results. In Sec. IV we review the $3N$ scattering formalism and give a short description of the 3NFs used in this study. Our experimental results are compared with the theoretical predictions in Sec. V. Summary and conclusions follow in Sec. VI.

## II. EXPERIMENTAL PROCEDURE

The cross section and a complete set of deuteron analyzing powers were measured with the SMART magnetic spectrograph [45] at the RIKEN Accelerator Research Facility. Part of the data was also obtained with a beam line polarimeter. Details of the experimental procedure together with the data reduction, when a beam line polarimeter is used, are described in Ref. [46]. In the following subsections we mainly present a description of the experimental procedure when the magnetic spectrograph is used.

### A. Polarized deuteron beams and target

The vector and tensor polarized deuteron beams were provided by the atomic beam type RIKEN polarized ion source [43]. The deuteron vector ($P_Z$) and tensor ($P_{ZZ}$) beam polarizations are given in terms of the occupation probabilities $N_+$, $N_0$, and $N_-$ of different deuteron spin magnetic substates $+1$, 0, and $-1$, respectively, by

$$P_Z=N_+-N_-, \tag{1}$$

$$P_{ZZ}=1-3N_0. \tag{2}$$

In the present measurements data were taken with the polarization modes of the polarized and unpolarized deuteron beams given in terms of the theoretical maximum polarization values as $(P_Z,P_{ZZ})=(0,0)$, $(0,-2)$, $(-2/3,0)$, and $(1/3,1)$. These polarization modes were changed cyclically at intervals of 5 s by switching the rf transition units of the ion source. In the measurements actual magnitudes of the beam polarizations were 60–80 % of the theoretical maximum values. After the acceleration of the deuterons by the AVF and Ring cyclotrons up to 140, 200, and 270 MeV the beam intensity was 0.1–10 nA. The deuteron polarization axis was rotated by a spin rotation Wien filter system [44] downstream of the polarized ion source, so that it was directed normally to the scattering plane for the measurement of $A_y^d$ and $A_{yy}$. In case of $A_{xx}$ the rotation was performed into the scattering plane so that the polarization axis pointed sideways, perpendicular to the beam direction. For the $A_{xz}$ measurement the spin symmetry axis was additionally rotated in the reaction plane and was aligned at an angle $\beta$ to the beam direction. The typical values of $\beta$ were $51.2°\pm0.5°$, $132.2°\pm0.5°$, and $41.1°\pm0.7°$ for 140, 200, and 270 MeV, respectively.

The polyethylene ($CH_2$) was employed as a hydrogen target ($^1$H). The target thickness was 29.7 mg/cm$^2$ for 140 MeV, 90.0 mg/cm$^2$ for 200 MeV, and 46.7 mg/cm$^2$ for 270 MeV.

### B. Beam line polarimeter

The beam polarization was monitored by two sets of beam line polarimeters. The first, the D-room polarimeter, was installed downstream of the Ring cyclotron. It was used for determination of the beam polarization after the deuterons were accelerated by the Ring cyclotron. The second, the swinger polarimeter (see Fig. 1), was placed in front of the scattering chamber in the experimental room. Since we rotated the incident beam direction by using the beam-swinger system of the SMART spectrograph in this measurement (see Sec. II C), the polarization axis of the beam was precessed during the beam transportation from the D-room polarimeter to the target position. The swinger polarimeter moved with the beam swinger so that this polarimeter could measure directly the beam polarization at the target. We monitored the beam polarization before and after the measurement by using the swinger polarimeter.

The polarimetry was made by using the known analyzing powers for the $d$–$p$ elastic scattering [46,51]. A $CH_2$ sheet was used as a target for each polarimeter. The target thickness was 90 mg/cm$^2$ at 140 and 200 MeV, and 270 mg/cm$^2$ at 270 MeV for the D-room polarimeter. For the swinger polarimeter the thickness was 90 mg/cm$^2$ at all three energies. Each polarimeter consisted of four pairs of plastic scintillators with a thickness of 1 cm placed symmetrically in left, right, up, and down directions. The scattered deuterons and recoil protons were detected in a kinematical coincidence. Such a setup allowed us to eliminate background events due to the deuteron breakup process or the inelastic scattering from carbon nuclei.

### C. SMART magnetic spectrograph and data acquisition processing

The SMART magnetic spectrograph [45] consists of a beam swinger and a cascade-type magnetic analyzer with two focal planes (see Fig. 1). The three-quadrupole and the two-dipole magnet sets in a QQDQD configuration serve as a high-resolution spectrometer with $p/\Delta p=13000$ offering the

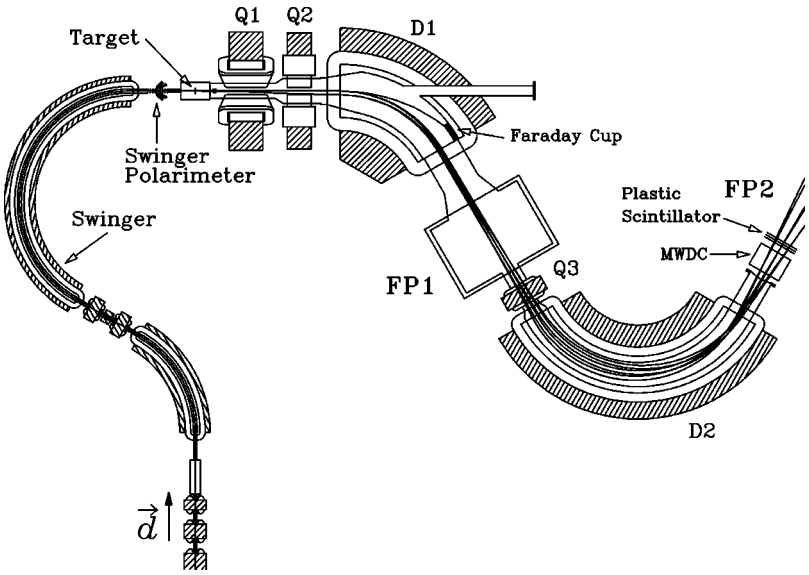


FIG. 1. Arrangement of the RIKEN SMART spectrograph. FP1 and FP2 denote the first and second focal planes, respectively. Scattered particles were momentum analyzed by the SMART spectrograph and detected at the second focal plane. The beam charge for the measurement at $\theta_{\mathrm{lab}}=0°$ ($\theta_{\mathrm{c.m.}}=180°$) was collected by the Faraday cup at the high momentum side of the dipole magnet D1.

second focal plane, at which the full angular acceptance is 200 $\mathrm{mrad}^V \times 50$ $\mathrm{mrad}^H$ (10 msr).

The polarized deuteron beams bombarded the $CH_2$ target placed in the scattering chamber. The incident beam direction was rotated by the swinger magnet, enabling us to measure the angular distribution without rotating the magnetic spectrograph. Note that the reaction plane of the SMART spectrograph is vertical because of this beam-swinger system. Scattered particles were momentum analyzed by the magnetic spectrograph and detected by a multiwire drift chamber (MWDC) and three plastic scintillators placed at the second focal plane. Depending on the scattering angle, the scattered deuterons (forward scattering $\theta_{\mathrm{c.m.}} \leqslant 90°$) or the recoil protons (backward scattering $\theta_{\mathrm{c.m.}} \geqslant 90°$) were detected by changing the magnetic field of the spectrograph.

The MWDC was used for the reconstruction of the particle trajectory. Its configuration is $X$-$Y$-$X'$-$Y'$-$X'$-$Y'$-$X$-$Y$, with the coordinate frames defined as follows. The $z$ axis refers to the central ray. The $x$ axis lies normal to the $z$ axis in the horizontal plane and the $y$ axis is taken as $\hat{\mathbf{x}} \times \hat{\mathbf{z}}$. All position sensitive planes are normal to the $z$ axis and separated by a distance of 50 mm from adjacent planes. The planes with primes are a half cell displaced relative to the unprimed ones, which helps to solve the left-right ambiguity. The cell size was 20 mm$\times$20 mm for the $X$ plane and 10 mm$\times$10 mm for the $Y$ plane.

The BICRON BC-408 plastic scintillators of the size 180 $\mathrm{mm}^H \times 800$ $\mathrm{mm}^W \times 5$ $\mathrm{mm}^T$ were used to generate an event trigger and their light outputs were used for particle identification (see Sec. III A). The photomultiplier Hamamatsu H1161 tubes were put on both ends of the scintillators via light guides. Figure 2 shows typical two-dimensional plots of scintillator detector light output at forward and backward scattering for the measurement performed at 270 MeV. When recoil protons were detected [shown in Fig. 2(b)], the background deuterons coming from inelastic deuteron scattering on $^{12}$C nuclei occupied a larger part of the spectra than the protons. However, the scintillation light output of deuterons was distinctly larger than that

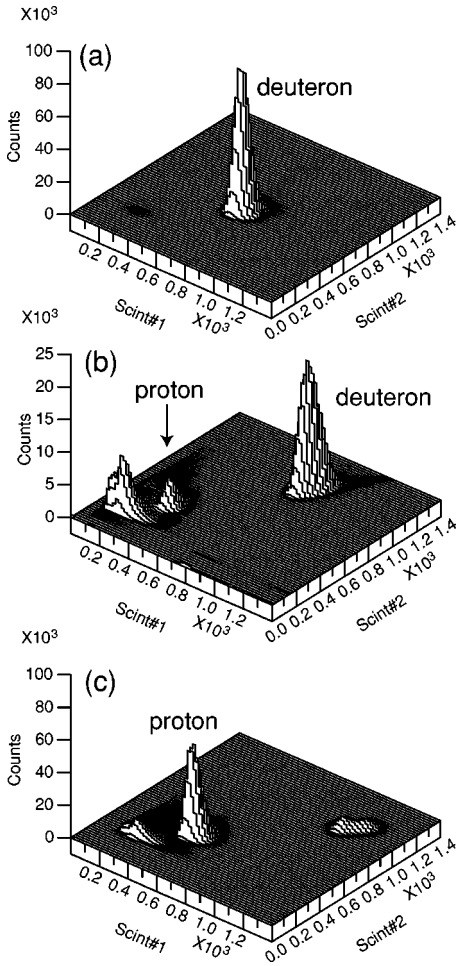


FIG. 2. Two-dimensional plot of scintillator detector light output for (a) forward scattering, and (b),(c) backward scattering. In (c) the background deuterons from inelastic scattering on $^{12}$C were eliminated using a hardware window gate.

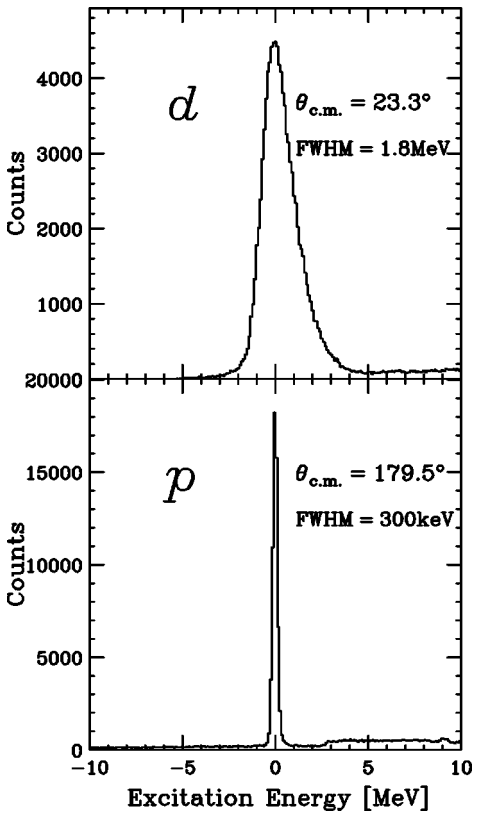


FIG. 3. Excitation energy spectra at $\theta_{\text{c.m.}}=23.3°$ (forward scattering) and at $\theta_{\text{c.m.}}=179.5°$ (backward scattering).

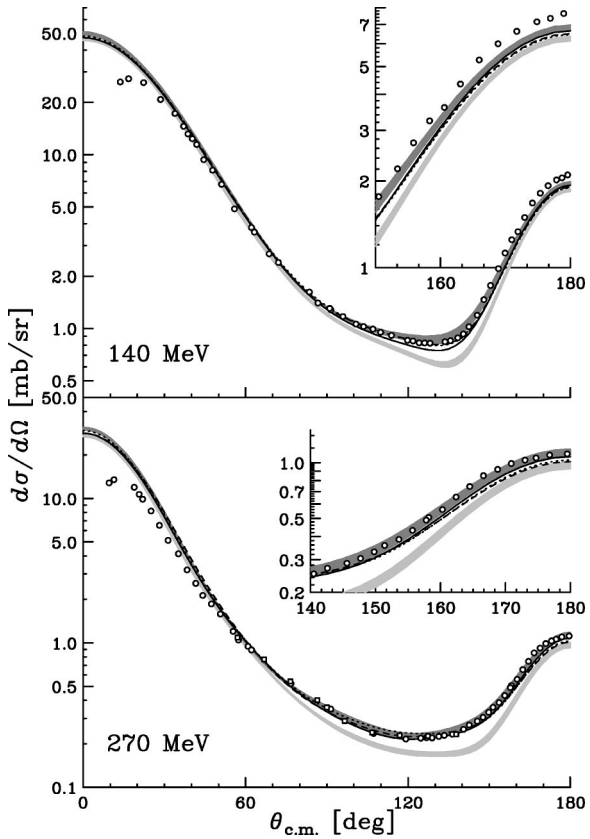


FIG. 4. The differential cross section $d\sigma/d\Omega$ in elastic $Nd$ scattering at $E_d=140$ and 270 MeV. The light shaded bands contain $NN$ force predictions (AV18, CD-Bonn, Nijm I, II, and 93), the dark shaded bands contain the $NN$ + TM 3NF predictions. The solid, short-dashed, and long-dashed lines are the AV18 + Urbana IX, CD-Bonn + TM′, and AV18 + Urbana IX + phenomenological spin-orbit 3NF predictions, respectively.

of protons. Thus a hardware window gate for the light output allowed us to eliminate the background deuterons, as shown in Fig. 2(c).

The beam charge for the measurement at $\theta_{\text{lab}}=0°$ ($\theta_{\text{c.m.}}=180°$) was collected by a Faraday cup installed at the high momentum side of the dipole magnet D1 (see Fig. 1). At other angles ($\theta_{\text{lab}}\geqslant 3°$) the beam charge was collected by a Faraday cup placed in the scattering chamber.

In order to get an accurate scattering angle, ion optical information was needed. For the present measurement the ion optical data for the SMART magnetic spectrograph were taken at three magnetic field strengths, corresponding to three deuteron momenta of 1042, 520, and 369 MeV/$c$. A sieve-type collimator (small holes in grid pattern) was applied to calibrate the trajectory in order to reconstruct the scattering angles. The $^{197}$Au$(d,d)$ elastic scattering at $E_d=270$ MeV was used for the strongest magnetic field calibration, while the $^{197}$Au$(p,p)$ reaction with $H_2^+$ beams accelerated to $E_p=135$ and 70 MeV was used for the two lower magnetic field calibrations. The thickness of the Au target was 60 $\mu$m. From these measurements, the angular resolutions of 3.3 and 3.8 mrad were obtained for the horizontal and vertical planes, respectively.

## III. DATA ANALYSIS AND EXPERIMENTAL RESULTS

### A. Cross section

Figure 3 shows energy spectra at $\theta_{\text{c.m.}}=23.3°$ (forward scattering) and at $\theta_{\text{c.m.}}=179.5°$ (backward scattering) for the measurement at 270 MeV. At forward scattering, the main source of background were the deuterons inelastically scattered on carbon nuclei. For backward scattering the main background were the protons produced in the deuteron breakup processes. The physical yields of the $d$-$p$ elastic scattering were obtained by subtracting the background yields approximated with a third-order polynomial.

The experimental results are shown in Fig. 4 and Tables I–III. The open circles in the figure are the experimental data obtained with the SMART spectrograph, while the open squares are the data obtained by using the D-room polarimeter. The errors shown in the figure and the tables are statistical only and are smaller than 1.3%. The ambiguity of the background subtraction for the excitation energy spectrum was estimated to be 3% at most.

### B. Determination of the absolute values of the cross section

It is essential to get precise absolute values of the cross section to compare with the state of the art Faddeev calculations. However, it is usually difficult to know experimentally the systematic uncertainty. We tried, therefore, to estimate the systematic uncertainty by comparing a cross section mea-

TABLE I. The data table for the *d-p* elastic scattering cross section at $E_d^{\rm lab}=140$ MeV obtained with the SMART spectrograph.

| $\theta_{\rm c.m.}$ (deg) | $(d\sigma/d\Omega)$ (mb/sr) | $\Delta(d\sigma/d\Omega)$ (mb/sr) |
|---|---|---|
| 13.7 | 26.175 | 0.057 |
| 16.8 | 27.313 | 0.058 |
| 22.4 | 25.950 | 0.061 |
| 28.6 | 20.752 | 0.049 |
| 33.9 | 17.247 | 0.041 |
| 37.1 | 14.537 | 0.039 |
| 40.3 | 12.345 | 0.039 |
| 38.7 | 13.150 | 0.038 |
| 41.9 | 11.446 | 0.037 |
| 44.5 | 9.352 | 0.017 |
| 47.8 | 8.133 | 0.017 |
| 51.2 | 6.744 | 0.014 |
| 55.9 | 4.870 | 0.010 |
| 55.9 | 4.870 | 0.010 |
| 63.3 | 3.580 | 0.013 |
| 72.1 | 2.394 | 0.007 |
| 68.7 | 2.685 | 0.012 |
| 62.2 | 3.805 | 0.010 |
| 83.6 | 1.619 | 0.006 |
| 86.7 | 1.398 | 0.004 |
| 91.0 | 1.303 | 0.009 |
| 91.6 | 1.276 | 0.004 |
| 96.0 | 1.170 | 0.006 |
| 100.8 | 1.059 | 0.008 |
| 103.6 | 1.024 | 0.004 |
| 107.0 | 0.990 | 0.004 |
| 109.9 | 0.950 | 0.003 |
| 113.9 | 0.911 | 0.004 |
| 119.8 | 0.854 | 0.004 |
| 121.8 | 0.846 | 0.004 |
| 124.1 | 0.826 | 0.004 |
| 126.1 | 0.824 | 0.004 |
| 128.2 | 0.821 | 0.004 |
| 133.7 | 0.838 | 0.003 |
| 135.7 | 0.850 | 0.003 |
| 138.4 | 0.882 | 0.004 |
| 140.4 | 0.928 | 0.004 |
| 142.5 | 1.022 | 0.004 |
| 145.6 | 1.190 | 0.004 |
| 148.0 | 1.463 | 0.005 |
| 150.5 | 1.765 | 0.005 |
| 153.4 | 2.204 | 0.009 |
| 155.9 | 2.713 | 0.009 |
| 158.3 | 3.236 | 0.010 |
| 160.6 | 3.601 | 0.017 |
| 163.1 | 4.345 | 0.016 |
| 166.0 | 5.266 | 0.017 |
| 168.8 | 5.996 | 0.018 |
| 171.7 | 6.622 | 0.019 |
| 174.8 | 7.149 | 0.032 |
| 176.9 | 7.347 | 0.032 |
| 179.0 | 7.637 | 0.038 |

TABLE II. The data table for the *d-p* elastic scattering cross section at $E_d^{\rm lab}=270$ MeV with the D-room polarimeter.

| $\theta_{\rm c.m.}$ (deg) | $(d\sigma/d\Omega)$ (mb/sr) | $\Delta(d\sigma/d\Omega)$ (mb/sr) |
|---|---|---|
| 57.0 | 1.088 | 0.012 |
| 66.8 | 0.766 | 0.006 |
| 76.6 | 0.541 | 0.004 |
| 86.5 | 0.401 | 0.003 |
| 90.0 | 0.357 | 0.003 |
| 96.6 | 0.288 | 0.005 |
| 106.7 | 0.240 | 0.003 |
| 116.9 | 0.228 | 0.004 |
| 127.3 | 0.227 | 0.002 |
| 137.8 | 0.233 | 0.003 |

sured at our facility to one known precisely. For this purpose we used the *pp* elastic scattering for which very reliable data sets exist.

The *pp* scattering experiment was carried out in the following manner to minimize the systematic uncertainties.

(1) When we finished the *d-p* scattering measurements at $E_d=270$ (140) MeV, we immediately changed the beam from deuteron to proton. This was possible since we used the $H_2{}^+$ ion as the proton beam. The mass of $H_2{}^+$ is almost identical to that of the deuteron so that we did not need to change any parameters of the accelerators or beam transport system. Note that $E_{H_2{}^+}=270$ (140) MeV corresponds to $E_p=135$ (70) MeV.

(2) Then we measured the *pp* cross section by using the same $CH_2$ target, the same beam charge collection system, and the same detection system, which were just used in the previous *d-p* measurement. Only the magnetic field of the SMART spectrograph had to be lowered to match the *pp* scattering kinematic condition.

(3) Finally we deduced the *pp* elastic cross sections $(d\sigma/d\Omega)_{\rm meas}$ and compared them with the values in the literature. Actually we used the cross section $(d\sigma/d\Omega)_{\rm calc}$ calculated by the phase-shift analysis program SAID [52] based on the large *NN* data basis.

The ratios of $(d\sigma/d\Omega)_{\rm meas}/(d\sigma/d\Omega)_{\rm calc}$ at 270 MeV are plotted in Fig. 5 for three measured angles. The average value is $1.010\pm0.013$. At 140 MeV the measured cross section is also consistent with the calculated ones. These results clearly show that we can measure the *pp* cross section to an accuracy of 2%, indicating a very small systematic uncertainty. Therefore we conclude that the present *d-p* cross section also involves just the similar size of systematic uncertainty, i.e., $<2\%$. This high accuracy is the most characteristic feature of our data. This conclusion is also supported by the fact that the cross sections measured by the SMART spectrograph and those by the D-room polarimeter agree with each other within the statistical uncertainties for overlapping angles.

### C. Analyzing powers

The spin-dependent *d-p* elastic scattering cross section for the polarized deuteron beam expressed in units of the unpolarized cross section is given by

TABLE III. The data table for the $d$-$p$ elastic scattering cross sections at $E_d^{\rm lab}=270$ MeV obtained with the SMART spectrograph.

| $\theta_{\rm c.m.}$ (deg) | $(d\sigma/d\Omega)$ (mb/sr) | $\Delta(d\sigma/d\Omega)$ (mb/sr) |
|---|---|---|
| 9.6 | 12.818 | 0.067 |
| 11.4 | 13.494 | 0.069 |
| 18.9 | 11.950 | 0.066 |
| 20.7 | 10.683 | 0.062 |
| 22.0 | 9.877 | 0.024 |
| 25.1 | 8.187 | 0.022 |
| 28.2 | 6.515 | 0.020 |
| 31.4 | 5.128 | 0.018 |
| 35.2 | 4.140 | 0.014 |
| 38.4 | 3.202 | 0.012 |
| 41.6 | 2.582 | 0.011 |
| 44.2 | 2.130 | 0.007 |
| 47.4 | 1.860 | 0.006 |
| 50.7 | 1.584 | 0.006 |
| 55.4 | 1.202 | 0.005 |
| 57.4 | 1.046 | 0.004 |
| 60.9 | 0.947 | 0.003 |
| 62.2 | 0.893 | 0.003 |
| 76.8 | 0.522 | 0.006 |
| 91.5 | 0.348 | 0.003 |
| 107.3 | 0.236 | 0.003 |
| 119.2 | 0.216 | 0.002 |
| 124.7 | 0.219 | 0.001 |
| 126.8 | 0.221 | 0.001 |
| 128.9 | 0.220 | 0.001 |
| 131.4 | 0.225 | 0.001 |
| 133.4 | 0.229 | 0.001 |
| 136.4 | 0.233 | 0.002 |
| 140.5 | 0.252 | 0.002 |
| 142.6 | 0.270 | 0.002 |
| 145.6 | 0.287 | 0.002 |
| 147.7 | 0.305 | 0.002 |
| 149.8 | 0.331 | 0.002 |
| 151.4 | 0.358 | 0.003 |
| 153.6 | 0.386 | 0.003 |
| 155.7 | 0.432 | 0.003 |
| 157.8 | 0.490 | 0.003 |
| 158.2 | 0.507 | 0.004 |
| 160.3 | 0.559 | 0.004 |
| 162.4 | 0.653 | 0.004 |
| 164.5 | 0.744 | 0.004 |
| 166.6 | 0.851 | 0.005 |
| 168.8 | 0.920 | 0.005 |
| 170.9 | 0.989 | 0.005 |
| 173.0 | 1.032 | 0.005 |
| 174.7 | 1.060 | 0.007 |
| 176.8 | 1.100 | 0.005 |
| 179.5 | 1.115 | 0.014 |

$$X=\sigma/\sigma_o=1+\frac{3}{2}p_yA_y^d+\frac{2}{3}p_{xz}A_{xz}+\frac{1}{3}(p_{xx}A_{xx}+p_{yy}A_{yy}+p_{zz}A_{zz}). \quad (3)$$

We rotated the spin direction to the $y$ axis for $A_y^d$ and $A_{yy}$, and to the $x$ axis for the $A_{xx}$ measurement. For the $A_{xz}$ measurement the spin symmetry axis was rotated into the reaction plane and inclined at the angle $\beta$ to the beam direction. Thus, the $X$ value was given as

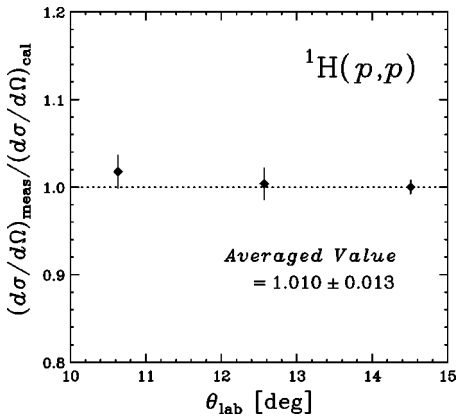


FIG. 5. Ratios of the measured cross section for $pp$ elastic scattering at 135 MeV to the calculated results by the SAID code.

$$X=1+\frac{3}{2}p_yA_y^d+\frac{1}{2}p_{yy}A_{yy} \quad \text{for } A_y^d \text{ and } A_{yy}, \quad (4)$$

$$X=1+\frac{1}{2}p_{xx}A_{xx} \quad \text{for } A_{xx}, \quad (5)$$

$$X=1+\frac{2}{3}p_{xz}A_{xz}+\frac{1}{3}(p_{xx}-p_{zz})A_{xx}+\frac{1}{3}(p_{yy}-p_{zz})A_{yy} \quad \text{for } A_{xz}, \quad (6)$$

with

$$A_{xx}+A_{yy}+A_{zz}=0.$$

It is clear that the $A_{xz}$ value was extracted by using the measured $A_{xx}$ and $A_{yy}$ values. All analyzing powers were determined by using the yields for three beam polarization modes described in Sec. II A.

The experimental results for the analyzing powers $A_y^d$, $A_{yy}$, $A_{xx}$, and $A_{xz}$ are shown in Figs. 6 and 7 and in Tables IV–VIII. The open circles in the figures are the experimental data obtained with the SMART spectrograph, while the open squares are the data obtained with the D-room polarimeter. The uncertainties shown are only statistical. For all deuteron analyzing powers at all three energies their absolute magnitudes do not go beyond 0.03 with the exception of $A_{xz}$ at 270 MeV obtained with the D-room polarimeter. There the error bars are larger (see Table V). The uncertainties for the analyzing powers coming from the background in the excitation energy spectrum were estimated as described in the following. The deuteron or proton yields were obtained by integrating the energy spectra of the particles around the peak region. In order to see the effect of the background in the spectrum, the integration range for a peak was changed systematically from the full width at 1/70 maximum to the full width at half maximum. The asymmetry results changed by 0.005 or less. Thus the systematic uncertainties did not over-

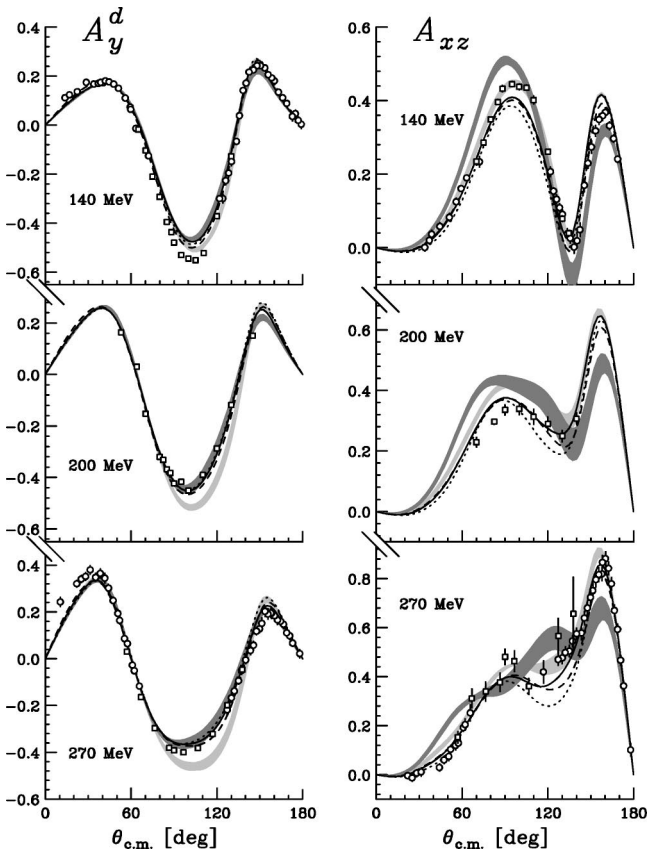


FIG. 6. The vector analyzing power $A_y^d$ and the tensor analyzing power $A_{xz}$ in elastic $Nd$ scattering at $E_d = 140$, 200, and 270 MeV. For the description of bands and curves see Fig. 4.

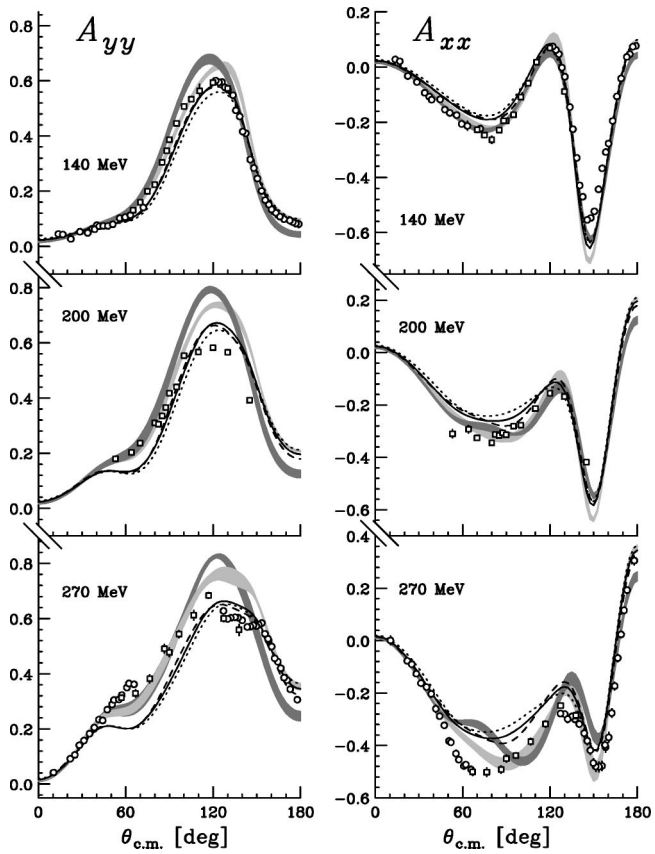


FIG. 7. The tensor analyzing powers $A_{yy}$ and $A_{xx}$ in elastic $Nd$ scattering at $E_d = 140$, 200, and 270 MeV. For the description of bands and curves see Fig. 4.

ride the statistical ones. The integration range of the width at 1/20 maximum was typically adopted to extract the final asymmetry. It should be noted that the two independent measurements provide almost the same results so the systematic errors due to the detection setup for all the deuteron analyzing powers and the cross section are small.

## IV. THEORETICAL FORMALISM AND DYNAMICAL INPUT

$Nd$ elastic scattering is described with the initial state $\phi$ composed of the deuteron and a momentum eigenstate of the nucleon. The outgoing state $\phi'$ corresponds to a changed outgoing nucleon-deuteron relative momentum. From the matrix element of the elastic scattering transition operator $U$,

$$\langle \phi' | U | \phi \rangle = \langle \phi' | P G_0^{-1} + V_4^{(1)}(1+P) + PT + V_4^{(1)}(1+P) G_0 T | \phi \rangle, \tag{7}$$

the various spin observables and the differential cross section are calculated [16,53]. In Eq. (7) $G_0$ is the free $3N$ propagator and $P$ takes into account the identity of the nucleons and is the sum of a cyclical and an anticyclical permutation of three nucleons. $V_4^{(1)}$ is one of the three contributions to the $3N$ force $V_4$,

$$V_4 = V_4^{(1)} + V_4^{(2)} + V_4^{(3)}, \tag{8}$$

where each $V_4^{(i)}$ is symmetrical under the exchange of the nucleons $jk$ with $j \neq i \neq k$. In the $2\pi$-exchange 3NF $V_4^{(i)}$ is a contribution to the $3N$ potential coming from (off-shell) rescattering of a pion on nucleon $i$. The first term in Eq. (7) is the well known single-nucleon exchange contribution and is followed by a single interaction of three-nucleons via a three-nucleon force. The remaining parts result from rescattering among three nucleons induced by two- and three-nucleon forces. All these rescatterings are summed up in the integral equation for the amplitude $T$ [16,54]:

$$T = tP\phi + (1+tG_0)V_4^{(1)}(1+P)\phi + tPG_0T + (1+tG_0)V_4^{(1)}(1+P)G_0T, \tag{9}$$

where the $NN$ $t$ operator is denoted by $t$. After projecting on a partial wave momentum space basis, this equation leads to a system of coupled integral equations, which can be solved numerically exactly for any nuclear force. In this study we restricted our partial wave basis taking all states with the total angular momenta $j \leqslant 5$ in the two-nucleon subsystem. This corresponds to a maximal number of 142 partial wave states in the $3N$ system for a given total angular momentum and guarantees converged results for the elastic scattering observables at the energies of the present paper. We checked

TABLE IV. The data table for the $d$-$p$ elastic scattering analyzing powers at $E_d^{\rm lab}=140$ MeV obtained with the SMART spectrograph.

| $\theta_{\rm c.m.}$ (deg) | $A_y^d$ | $\Delta A_y^d$ | $A_{yy}$ | $\Delta A_{yy}$ | $A_{xx}$ | $\Delta A_{xx}$ | $A_{xz}$ | $\Delta A_{xz}$ |
|---|---|---|---|---|---|---|---|---|
| 13.7 | 0.112 | 0.007 | 0.045 | 0.003 | 0.028 | 0.002 | | |
| 16.8 | 0.124 | 0.007 | 0.043 | 0.003 | 0.021 | 0.002 | | |
| 22.4 | 0.137 | 0.008 | 0.027 | 0.003 | −0.032 | 0.002 | | |
| 28.6 | 0.175 | 0.008 | 0.053 | 0.003 | −0.054 | 0.003 | | |
| 33.9 | 0.168 | 0.007 | 0.049 | 0.002 | −0.093 | 0.003 | 0.001 | 0.010 |
| 37.1 | 0.171 | 0.008 | 0.064 | 0.003 | −0.107 | 0.003 | 0.020 | 0.010 |
| 40.3 | 0.173 | 0.009 | 0.077 | 0.003 | | | | |
| 38.7 | 0.175 | 0.009 | 0.062 | 0.003 | −0.118 | 0.003 | 0.037 | 0.011 |
| 41.9 | 0.181 | 0.009 | 0.073 | 0.003 | | | | |
| 44.5 | 0.177 | 0.005 | 0.074 | 0.002 | −0.117 | 0.003 | 0.058 | 0.011 |
| 47.8 | 0.168 | 0.006 | 0.074 | 0.002 | −0.154 | 0.003 | | |
| 51.2 | 0.151 | 0.006 | 0.080 | 0.002 | −0.166 | 0.004 | 0.083 | 0.011 |
| 55.9 | 0.111 | 0.006 | 0.102 | 0.002 | −0.174 | 0.003 | 0.125 | 0.010 |
| 59.4 | 0.074 | 0.006 | 0.104 | 0.002 | −0.206 | 0.003 | 0.161 | 0.007 |
| 59.7 | 0.065 | 0.009 | 0.106 | 0.003 | | | | |
| 63.3 | −0.013 | 0.009 | 0.113 | 0.003 | −0.213 | 0.017 | 0.190 | 0.007 |
| 72.1 | −0.125 | 0.007 | 0.141 | 0.002 | −0.223 | 0.005 | 0.234 | 0.015 |
| 121.8 | −0.299 | 0.010 | 0.601 | 0.002 | 0.075 | 0.003 | 0.207 | 0.013 |
| 124.1 | −0.299 | 0.019 | 0.595 | 0.004 | 0.062 | 0.004 | 0.154 | 0.009 |
| 126.1 | −0.226 | 0.017 | 0.596 | 0.004 | 0.047 | 0.004 | 0.132 | 0.012 |
| 128.2 | −0.195 | 0.018 | 0.577 | 0.004 | −0.002 | 0.004 | 0.109 | 0.011 |
| 130.2 | −0.148 | 0.018 | 0.568 | 0.004 | −0.035 | 0.007 | 0.091 | 0.012 |
| 133.7 | −0.066 | 0.013 | 0.548 | 0.003 | −0.145 | 0.003 | 0.038 | 0.014 |
| 135.7 | 0.039 | 0.012 | 0.493 | 0.003 | −0.225 | 0.003 | 0.026 | 0.014 |
| 138.4 | 0.142 | 0.011 | 0.471 | 0.003 | −0.329 | 0.005 | 0.002 | 0.017 |
| 140.4 | 0.172 | 0.009 | 0.416 | 0.002 | −0.429 | 0.005 | 0.019 | 0.018 |
| 142.5 | 0.217 | 0.009 | 0.410 | 0.002 | −0.470 | 0.005 | 0.049 | 0.019 |
| 145.6 | 0.226 | 0.008 | 0.315 | 0.003 | −0.554 | 0.004 | 0.170 | 0.018 |
| 148.0 | 0.243 | 0.007 | 0.284 | 0.003 | −0.547 | 0.004 | 0.230 | 0.014 |
| 150.5 | 0.243 | 0.007 | 0.246 | 0.003 | −0.523 | 0.003 | 0.274 | 0.017 |
| 153.4 | 0.234 | 0.008 | 0.201 | 0.003 | −0.443 | 0.004 | 0.318 | 0.015 |
| 155.9 | 0.206 | 0.008 | 0.168 | 0.003 | −0.367 | 0.004 | 0.349 | 0.014 |
| 158.3 | 0.193 | 0.007 | 0.152 | 0.003 | −0.308 | 0.003 | 0.359 | 0.013 |
| 160.2 | 0.181 | 0.009 | 0.134 | 0.016 | −0.277 | 0.004 | 0.368 | 0.013 |
| 163.1 | 0.135 | 0.009 | 0.122 | 0.018 | −0.195 | 0.003 | 0.332 | 0.011 |
| 166.0 | 0.112 | 0.008 | 0.108 | 0.003 | −0.106 | 0.003 | 0.297 | 0.010 |
| 168.8 | 0.089 | 0.008 | 0.099 | 0.003 | −0.041 | 0.003 | 0.241 | 0.009 |
| 172.8 | 0.036 | 0.019 | 0.094 | 0.013 | 0.037 | 0.006 | | |
| 174.8 | 0.047 | 0.015 | 0.088 | 0.012 | 0.047 | 0.006 | | |
| 176.9 | 0.020 | 0.015 | 0.083 | 0.011 | 0.074 | 0.005 | | |
| 179.0 | 0.004 | 0.017 | 0.081 | 0.013 | 0.077 | 0.006 | | |

that convergence has been achieved by looking at the results obtained when including $j=6$ states, which increases the number of states to 194. This convergence check was done without 3NF. The inclusion of a 3NF has been carried through for all total angular momenta of the 3$N$ system up to $J=13/2$ while the longer ranged 2$N$ interactions require states up to $J=25/2$. For the details of the formalism and the numerical performance we refer to Refs. [14–16].

In this paper we show calculations with various combinations of *NN* and 3NF forces. The AV18, CD-Bonn, Nijm I, II and 93 forces are the *NN* forces and the TM 3NF, a modified version thereof labeled as TM′, and the Urbana IX force are the 3NFs. In addition, we show the effects of a phenomenological spin-orbit 3NF that is added to the AV18 + Urbana IX combination.

We combined each of those *NN* interactions with the TM model [10,11], where the cutoff parameter $\Lambda$ in the strong form factor parametrization was adjusted to reproduce the $^3$H binding energy separately for each *NN* force [55]. The $\Lambda$ values in units of the pion mass $m_\pi$ are 5.215, 4.856, 5.120,

TABLE V. The data table for the $d$-$p$ elastic scattering analyzing powers at $E_d^{\rm lab}=140$ MeV obtained with the D-room polarimeter.

| $\theta_{\rm c.m.}$ (deg) | $A_y^d$ | $\Delta A_y^d$ | $A_{yy}$ | $\Delta A_{yy}$ | $A_{xx}$ | $\Delta A_{xx}$ | $A_{xz}$ | $\Delta A_{xz}$ |
|---|---|---|---|---|---|---|---|---|
| 65.0 | −0.018 | 0.002 | 0.131 | 0.003 | | | | |
| 70.1 | −0.103 | 0.003 | 0.160 | 0.003 | −0.227 | 0.004 | 0.234 | 0.005 |
| 75.0 | −0.210 | 0.003 | 0.200 | 0.004 | −0.247 | 0.004 | 0.286 | 0.004 |
| 80.0 | −0.293 | 0.006 | 0.223 | 0.008 | −0.263 | 0.013 | 0.349 | 0.006 |
| 85.0 | −0.394 | 0.004 | 0.304 | 0.005 | −0.228 | 0.005 | 0.397 | 0.007 |
| 88.2 | −0.436 | 0.004 | 0.347 | 0.005 | −0.194 | 0.007 | 0.433 | 0.009 |
| 90.0 | −0.479 | 0.004 | 0.387 | 0.005 | −0.195 | 0.009 | | |
| 95.0 | −0.530 | 0.005 | 0.446 | 0.005 | −0.173 | 0.005 | 0.446 | 0.008 |
| 100.0 | −0.544 | 0.004 | 0.507 | 0.005 | −0.109 | 0.004 | 0.438 | 0.008 |
| 105.0 | −0.552 | 0.005 | 0.534 | 0.006 | −0.058 | 0.005 | 0.436 | 0.008 |
| 110.7 | −0.522 | 0.007 | 0.564 | 0.025 | 0.018 | 0.005 | 0.402 | 0.011 |
| 120.0 | −0.371 | 0.006 | 0.594 | 0.007 | 0.070 | 0.006 | 0.261 | 0.006 |
| 130.0 | −0.127 | 0.008 | 0.573 | 0.008 | −0.089 | 0.009 | 0.079 | 0.008 |

5.072, and 5.212 for AV18, CD-Bonn, Nijm I, II, and 93, respectively [17].

The standard parametrization of the TM 3NF has been criticized in [22,23,50] on the basis that it violates chiral symmetry. A form more consistent with chiral symmetry has been proposed by modifying the $c$ term of the TM force and absorbing the long-range part of this term into the $a$ term, leading to its new value $a' \equiv a - 2m_\pi^2 c = -0.87/m_\pi$ [22,23,50], and rejecting the rest of the $c$ term. This new form is called TM$'$ and the corresponding $\Lambda$ value, when it is used with the CD-Bonn potential, is $\Lambda = 4.593 m_\pi$.

For the AV18 potential we also used the Urbana IX 3NF [12]. That force is based on the Fujita-Miyazawa assumption of an intermediate $\Delta$ excitation in the $2\pi$ exchange [9] and is augmented by a phenomenological spin- and isospin-independent short-range part. This force was formulated in configuration space [12]. For the partial wave decomposition of the Urbana IX 3NF in momentum space we refer to Ref. [17].

These three forces cover the present day 3NF models of $2\pi$-exchange nature. In the spirit of a meson-exchange picture one should also consider other two-meson exchanges such as $\pi$-$\rho$ and $\rho$-$\rho$. Such extensions have been developed [11,56] and in Ref. [57] applied in the $3N$ continuum. It is found that the effects of the $\pi$-$\rho$ exchange lead to a reduction of the effects caused by the $2\pi$-exchange TM 3NF. The effects induced by $\rho$-$\rho$ exchanges turned out to be negligible. This requires further investigation.

One of the observables considered here is the deuteron vector analyzing power $A_y^d$, for which an unusual large discrepancy between pure $2N$ force predictions and experimental data exist at low energies ($A_y$ puzzle) [16,19,20]. Attempts to improve the description of the low-energy vector analyzing powers with the $2\pi$-exchange 3NF failed

TABLE VI. The data table for the $d$-$p$ elastic scattering analyzing powers at $E_d^{\rm lab}=200$ MeV obtained with the D-room polarimeter.

| $\theta_{\rm c.m.}$ (deg) | $A_y^d$ | $\Delta A_y^d$ | $A_{yy}$ | $\Delta A_{yy}$ | $A_{xx}$ | $\Delta A_{xx}$ | $A_{xz}$ | $\Delta A_{xz}$ |
|---|---|---|---|---|---|---|---|---|
| 53.0 | 0.164 | 0.004 | 0.180 | 0.005 | −0.310 | 0.016 | | |
| 64.0 | 0.031 | 0.004 | 0.203 | 0.005 | −0.293 | 0.015 | | |
| 70.0 | −0.152 | 0.004 | 0.236 | 0.005 | −0.326 | 0.005 | 0.229 | 0.017 |
| 80.0 | −0.320 | 0.005 | 0.309 | 0.005 | −0.345 | 0.006 | | |
| 82.5 | −0.332 | 0.005 | 0.305 | 0.005 | −0.313 | 0.006 | 0.296 | 0.009 |
| 85.0 | −0.368 | 0.005 | 0.335 | 0.005 | −0.317 | 0.006 | | |
| 87.4 | −0.383 | 0.003 | 0.366 | 0.003 | −0.306 | 0.004 | | |
| 90.0 | −0.423 | 0.005 | 0.417 | 0.005 | −0.314 | 0.005 | 0.336 | 0.017 |
| 95.0 | −0.416 | 0.005 | 0.441 | 0.005 | −0.282 | 0.006 | | |
| 100.0 | −0.451 | 0.005 | 0.553 | 0.005 | −0.277 | 0.006 | 0.339 | 0.019 |
| 110.0 | −0.390 | 0.005 | 0.567 | 0.004 | −0.214 | 0.006 | 0.313 | 0.025 |
| 120.0 | −0.287 | 0.006 | 0.582 | 0.005 | −0.155 | 0.006 | 0.290 | 0.023 |
| 130.0 | −0.118 | 0.006 | 0.566 | 0.006 | −0.169 | 0.008 | 0.249 | 0.019 |
| 140.0 | | | | | | | 0.307 | 0.020 |
| 145.0 | 0.151 | 0.008 | 0.391 | 0.008 | −0.418 | 0.010 | | |

TABLE VII. The data table for the $d$-$p$ elastic scattering analyzing powers at $E_d^{\rm lab}=270$ MeV obtained with the SMART spectrograph.

| $\theta_{\rm c.m.}$ (deg) | $A_y^d$ | $\Delta A_y^d$ | $A_{yy}$ | $\Delta A_{yy}$ | $A_{xx}$ | $\Delta A_{xx}$ | $A_{xz}$ | $\Delta A_{xz}$ |
|---|---|---|---|---|---|---|---|---|
| 10.5 | 0.243 | 0.020 | 0.042 | 0.007 | 0.001 | 0.017 | | |
| 22.0 | 0.321 | 0.015 | 0.092 | 0.004 | −0.077 | 0.011 | −0.004 | 0.013 |
| 25.1 | 0.341 | 0.016 | 0.106 | 0.004 | −0.090 | 0.011 | −0.013 | 0.014 |
| 28.2 | 0.352 | 0.017 | 0.141 | 0.005 | −0.126 | 0.011 | 0.006 | 0.015 |
| 31.4 | 0.380 | 0.019 | 0.158 | 0.006 | −0.162 | 0.012 | 0.011 | 0.017 |
| 35.2 | 0.348 | 0.018 | 0.183 | 0.006 | −0.177 | 0.012 | | |
| 38.4 | 0.365 | 0.020 | 0.205 | 0.006 | −0.203 | 0.013 | | |
| 41.6 | 0.345 | 0.021 | 0.234 | 0.007 | −0.260 | 0.014 | | |
| 44.2 | 0.302 | 0.017 | 0.231 | 0.006 | −0.288 | 0.011 | 0.029 | 0.015 |
| 47.4 | 0.249 | 0.015 | 0.270 | 0.006 | −0.323 | 0.011 | 0.060 | 0.016 |
| 50.7 | 0.194 | 0.016 | 0.289 | 0.006 | −0.383 | 0.013 | 0.074 | 0.017 |
| 52.0 | 0.164 | 0.015 | 0.305 | 0.006 | −0.388 | 0.012 | 0.103 | 0.017 |
| 55.4 | 0.086 | 0.014 | 0.307 | 0.006 | −0.431 | 0.013 | 0.119 | 0.019 |
| 57.4 | 0.065 | 0.010 | 0.323 | 0.005 | −0.454 | 0.011 | 0.129 | 0.014 |
| 60.9 | −0.027 | 0.011 | 0.350 | 0.005 | −0.478 | 0.012 | 0.192 | 0.015 |
| 62.2 | −0.051 | 0.010 | 0.365 | 0.005 | −0.473 | 0.011 | 0.204 | 0.024 |
| 65.8 | −0.117 | 0.013 | 0.362 | 0.006 | −0.492 | 0.013 | 0.252 | 0.034 |
| 116.9 | | | | | | | 0.419 | 0.046 |
| 127.2 | −0.218 | 0.018 | 0.628 | 0.008 | −0.278 | 0.012 | 0.470 | 0.024 |
| 130.1 | −0.167 | 0.019 | 0.599 | 0.008 | −0.280 | 0.012 | 0.476 | 0.023 |
| 132.2 | −0.138 | 0.021 | 0.603 | 0.009 | −0.299 | 0.014 | 0.498 | 0.024 |
| 135.1 | −0.094 | 0.016 | 0.605 | 0.008 | −0.289 | 0.012 | 0.504 | 0.024 |
| 137.2 | −0.050 | 0.018 | 0.604 | 0.009 | −0.300 | 0.013 | 0.545 | 0.023 |
| 140.1 | −0.005 | 0.017 | 0.594 | 0.008 | −0.318 | 0.013 | 0.575 | 0.023 |
| 143.5 | 0.035 | 0.018 | 0.570 | 0.008 | −0.353 | 0.017 | 0.578 | 0.028 |
| 145.6 | 0.058 | 0.017 | 0.571 | 0.008 | −0.382 | 0.016 | 0.639 | 0.028 |
| 147.7 | 0.118 | 0.016 | 0.576 | 0.008 | −0.418 | 0.016 | 0.680 | 0.028 |
| 149.8 | 0.128 | 0.016 | 0.573 | 0.008 | −0.467 | 0.016 | 0.723 | 0.029 |
| 151.4 | 0.151 | 0.024 | 0.578 | 0.010 | −0.480 | 0.019 | 0.751 | 0.030 |
| 153.6 | 0.203 | 0.023 | 0.584 | 0.010 | −0.481 | 0.019 | 0.796 | 0.030 |
| 155.7 | 0.191 | 0.022 | 0.545 | 0.010 | −0.478 | 0.018 | 0.816 | 0.029 |
| 157.8 | 0.196 | 0.020 | 0.527 | 0.009 | −0.398 | 0.016 | 0.819 | 0.028 |
| 158.2 | 0.194 | 0.023 | 0.521 | 0.010 | −0.406 | 0.020 | 0.866 | 0.029 |
| 160.3 | 0.184 | 0.022 | 0.499 | 0.009 | −0.369 | 0.019 | 0.881 | 0.029 |
| 162.4 | 0.166 | 0.020 | 0.456 | 0.009 | −0.276 | 0.017 | 0.842 | 0.027 |
| 164.5 | 0.160 | 0.018 | 0.444 | 0.008 | −0.173 | 0.015 | 0.779 | 0.026 |
| 166.6 | 0.147 | 0.017 | 0.420 | 0.008 | −0.066 | 0.014 | 0.670 | 0.023 |
| 168.8 | 0.111 | 0.017 | 0.386 | 0.007 | 0.024 | 0.013 | 0.593 | 0.022 |
| 170.9 | 0.098 | 0.016 | 0.377 | 0.007 | 0.116 | 0.013 | 0.467 | 0.021 |
| 173.0 | 0.067 | 0.015 | 0.344 | 0.007 | 0.193 | 0.013 | 0.362 | 0.019 |
| 177.9 | 0.022 | 0.018 | 0.306 | 0.007 | 0.306 | 0.017 | 0.101 | 0.026 |

[16,17,19,58,59]. In Ref. [60] a phenomenological spin-orbit 3NF (SO-3NF) was introduced by modifying the $\vec{L}\cdot\vec{S}$ term of the *NN* potential with a two-parameter three-body function depending on the hyperradius $\rho$:

$$W_{\rm 3NF}^{\rm SO}=W_0 e^{-\alpha\rho}\sum_{i<j}\vec{L}_{ij}\cdot\vec{S}_{ij}P_{11}(ij). \tag{10}$$

Such a choice and the restriction to the isospin $t=1$ and spin $s=1$ states in the two-nucleon subsystem $ij$ through the use of the projection operator $P_{11}$ were guided by the fact that the low-energy vector analyzing powers show an extreme sensitivity to the $^3P_j$ *NN* force components. The strength $W_0$ and the range $\alpha$ were adjusted together with the AV18 potential to improve the description of the low-energy vector analyzing powers and to resolve the low-energy $A_y$ puzzle [60]. To check the effects caused by this phenomenological 3NF model at our energies we applied it together with the AV18 potential and the Urbana IX 3NF, taking the medium-range parameters of Ref. [60]: $\alpha=1.2$ fm$^{-1}$ and $W_0=$

TABLE VIII. The data table for the $d$-$p$ elastic scattering analyzing powers at $E_d^{\rm lab}=270$ MeV obtained with the D-room polarimeter.

| $\theta_{\rm c.m.}$ (deg) | $A_y^d$ | $\Delta A_y^d$ | $A_{yy}$ | $\Delta A_{yy}$ | $A_{xx}$ | $\Delta A_{xx}$ | $A_{xz}$ | $\Delta A_{xz}$ |
|---|---|---|---|---|---|---|---|---|
| 57.0 | 0.030 | 0.003 | 0.314 | 0.010 | | | 0.152 | 0.024 |
| 66.8 | −0.164 | 0.004 | 0.329 | 0.013 | −0.500 | 0.015 | 0.311 | 0.039 |
| 76.6 | −0.297 | 0.006 | 0.382 | 0.015 | −0.502 | 0.016 | 0.339 | 0.040 |
| 86.5 | −0.381 | 0.006 | 0.491 | 0.016 | −0.492 | 0.014 | 0.377 | 0.038 |
| 90.0 | −0.391 | 0.006 | 0.478 | 0.016 | −0.450 | 0.014 | 0.481 | 0.032 |
| 96.6 | −0.400 | 0.005 | 0.544 | 0.013 | −0.438 | 0.011 | 0.463 | 0.043 |
| 106.7 | −0.382 | 0.006 | 0.612 | 0.018 | −0.385 | 0.013 | 0.360 | 0.033 |
| 116.9 | −0.322 | 0.008 | 0.685 | 0.011 | −0.318 | 0.012 | | |
| 127.3 | −0.199 | 0.006 | 0.600 | 0.011 | −0.248 | 0.008 | 0.566 | 0.072 |
| 137.8 | −0.046 | 0.005 | 0.559 | 0.020 | −0.285 | 0.014 | 0.656 | 0.150 |

−10 MeV. For the momentum space representation of this SO-3NF we refer to Ref. [61].

## V. COMPARISON OF DATA WITH THEORETICAL PREDICTIONS

Figure 4 compares the unpolarized differential cross section data taken at $E_d^{\rm lab}=140$ and 270 MeV with the theoretical predictions. The various *NN* force predictions are very close to each other, forming a narrow band (light shaded bands in the figure), which reflects the weak dependence on the particular *NN* interaction used. They clearly underestimate the data for c.m. angles greater than 90°. Especially large differences up to 30% exist in the region of the minimum around $\theta_{\rm c.m.}=120°-140°$. At 270 MeV, the inclusion of the TM 3NF (the dark shaded band) leads to a good description of the data in the domain, where the cross section is minimal. The inclusion of the TM′ (short-dashed curve) and the Urbana IX (solid curve) 3NFs also lead to a good agreement to the data. Even in the very backward angles the TM 3NF (dark shaded band) or the Urbana IX (solid curve) 3*N* force provides a good description of the data, while the curve with the TM′ 3NF (short-dashed curve) deviates slightly from the data. At 140 MeV, the discrepancy in the cross section minimum is also removed by including 3NFs, however none of the 3NFs improves the agreement in the backward angles. The inclusion of the phenomenological SO-3NF (long-dashed curves) to the AV18 + Urbana IX prediction (solid curves) leads only to a minor modification at both energies. Note that the difference seen at forward angles $\theta_{\rm c.m.}\leqslant 30°$ is due to the neglect of the $pp$−Coulomb-force interaction in the calculations.

In Figs. 6 and 7 we compare the vector and tensor analyzing powers with different nuclear force predictions at 140, 200, and 270 MeV. For $A_y^d$ the light shaded bands for the *NN* force predictions are rather narrow at all three energies, and they become slightly wider with increasing energy. They clearly underestimate the $A_y^d$ data in the region of the $A_y^d$ minimum around $\theta_{\rm c.m.}=90°-130°$ at 200 and 270 MeV and overestimate the data at backward angles at 270 MeV. The inclusion of the TM 3NF (dark shaded bands) removes the clear discrepancy in the minimum as well as in the backward angles. In the case of the TM′ (short-dashed curves) or Urbana IX 3NF (solid curves), they also provide a reasonably good agreement to the data. The inclusion of the phenomenological SO-3NF (long-dashed curves) changes only slightly the AV18 + Urbana IX 3NF prediction (solid curves) at all three energies. At 140 MeV the very narrow light shaded band of the 2*N* force predictions follows the data except for the region around 100°. It is reported that at lower energies ($E/A\lesssim 20$ MeV) the $pp$ Coulomb force decreases the $A_y^d$ values significantly around the $A_y^d$ maximum region at 100° [18]. Assuming that this effect acts in the same direction at this energy the inclusion of the $pp$ Coulomb force would explain the above overestimation. In any case the result of the comparison between the data and the 2*N* force predictions at this energy is different from those at the two higher energies. The predicted effects of the 3NFs are rather small, leading to a small increase of $A_y^d$ in the region of the $A_y^d$ minimum, and they do not improve the agreement to the data. The TM (dark shaded band), TM′ (short-dashed curve), and Urbana IX (solid curve) 3NFs lead practically to the same results.

In the case of the tensor analyzing powers the situation is different and challenging. The spreads of 2*N* (light shaded) and 2*N*+TM-3NF (dark shaded) bands are wider than those for the cross section and $A_y^d$. At 140 MeV the 2*N* force predictions (light shaded band) show a moderate agreement to the data, which is destroyed with increasing energy. The data are not described by any type of 3NFs used. In most cases the description even deteriorates when such 3NFs are included. It is interesting to note that clear differences between various 3NF predictions appear at some angles, especially between the TM (dark shaded band) and other predictions. The TM′ (short-dashed curves) and Urbana IX (solid curves) 3NFs show in most cases similar effects for all tensor analyzing powers at all three energies. The SO-3NF (long-dashed curves) changes only slightly the AV18 + Urbana IX predictions (solid curves).

For $A_{xz}$ the 2*N* force predictions (light shaded band) agree quite well with the data at 140 and 270 MeV. At 200 MeV they overestimate the experimental data. The large effects of the TM force (dark shaded band) are not supported at every energy, while the smaller effects of the Urbana IX force

(solid curve) are most compatible with data. The effects of TM′ (short-dashed curve) act in a direction opposite to those of the TM (dark shaded bands) and they are too large around middle angles at 140 and 270 MeV.

For $A_{yy}$ all theoretical predictions have almost the same values and the data are well reproduced by them at forward angles $\theta_{\mathrm{c.m.}} \leqslant 40°$. At backward angles $\theta_{\mathrm{c.m.}} \geqslant 150°$, the TM force (dark shaded bands) is an exception and the data in this region support 2*N* (light shaded bands) and other 3NFs, the effects of which are small. A complicated picture of effects arises at intermediate angles. The 2*N* band (light shaded band) gives rather good description of the data at 140 MeV, but a difference between the data and the calculations exists persistently around $\theta_{\mathrm{c.m.}} = 120° - 150°$ and becomes larger with increasing energy. Such a deficiency is not removed by adding any of the 3NFs used. The difference between the 2*N* force predictions (light shaded bands) and the TM 3NF ones (dark shaded bands) becomes much more visible at the two higher energies; however, the inclusion of this 3NF shifts the predictions even further away from the data, especially around $\theta_{\mathrm{c.m.}} = 120° - 150°$. The TM′ (short-dashed curves) and Urbana IX (solid curves) 3NFs also fail to describe the data, although their predictions approach the data around $\theta_{\mathrm{c.m.}} = 120° - 150°$.

For $A_{xx}$, at 140 and 200 MeV the effects of the TM 3NF (dark shaded bands) are rather small and their bands as well as the *NN* one (light shaded bands) reproduce the data rather well. The TM′ (short-dashed curves) and Urbana IX (solid curves) models overestimate the data at intermediate angles. At 270 MeV and in the angular region $\theta_{\mathrm{c.m.}} = 50° - 150°$ all 3NFs used lead to large effects of different magnitude and direction. However, such effects are not supported by our data.

A quantitative determination of 3NF effects in terms of reduced $\chi^2$ values which are obtained by using statistical errors supports the above picture. In Fig. 8 we show the energy dependence of the reduced $\chi^2$ values for each observable in the angular range of $\theta_{\mathrm{c.m.}} = 60° - 180°$ for the cross section and analyzing powers. It is clearly seen that the cross section shows a drastic discrepancy between the data and the *NN* force only predictions (light shaded bands), and the agreement is significantly improved by considering 3NFs. The vector analyzing power $A_y^d$ reveals a similar behavior and the description of the data is also improved by adding 3NFs at the two higher energies. For the tensor analyzing powers no calculation is preferred and all of them are of a similar, unsatisfactory quality. Adding a 3NF does not improve drastically the description of the data. For $A_{xx}$, $A_{yy}$, and $A_{xz}$ at 270 MeV and for $A_{yy}$ and $A_{xz}$ at 200 MeV adding the TM 3NF (dark shaded bands) even worsens significantly the pure *NN* predictions. In conclusion, present tensor analyzing power data reveal deficiencies in the spin-dependent part of the present 3NF models.

## VI. SUMMARY AND CONCLUSIONS

We performed measurements of a complete set of deuteron analyzing powers at three intermediate energies $E_d^{\mathrm{lab}} = 140$, 200, and 270 MeV, covering a wide angular range

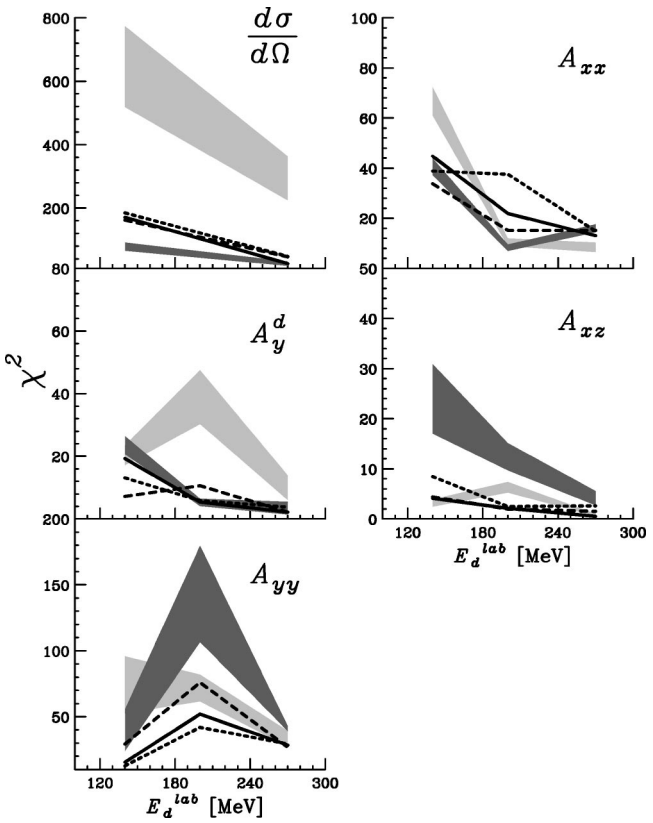


FIG. 8. Reduced $\chi^2$ values for the cross section and all deuteron analyzing powers ($A_y$, $A_{yy}$, $A_{xx}$, and $A_{xz}$) in the angular range of $\theta_{\mathrm{c.m.}} = 60° - 180°$ at $E_d^{\mathrm{lab}} = 140$, 200, and 270 MeV. For the description of bands and curves see Fig. 4.

$\theta_{\mathrm{c.m.}} = 10° - 180°$. In addition, at 140 and 270 MeV the unpolarized cross section was measured. High-precision data have been obtained. For all deuteron analyzing powers the statistical uncertainties are smaller than 0.03 at all three energies and the systematic uncertainties do not override the statistical errors. For the cross section the statistical errors are within 1.3% and the ambiguity of background subtraction is 3% at most. Also we tried to estimate the systematic uncertainties of the absolute cross section values for *d-p* elastic scattering by comparing the measured cross section for the *pp* elastic scattering to that of the calculated one by the SAID code. They are estimated to be less than 2%. In addition, the agreement of the analyzing power and the cross section data obtained in two independent measurements performed with different experimental arrangements gives confidence that the systematic errors due to the detection setup are small. These results show that our data are reliable.

Our data have been compared with predictions based on different nuclear forces in order to look for evidences of 3NF effects and to test present day 3NF models with respect to the effects that these forces cause. Based on the comparison of present data with pure 2*N* force predictions clear discrepancies have been found for most observables, especially in the middle angular range, which become larger with increasing energy. For the cross section these discrepancies can be removed by including all 3NFs used in the present paper: the TM 3NF, its modified version called TM′, and the Urbana

IX force. Such a behavior is also found for the vector analyzing power $A_y^d$ at 200 and 270 MeV. At 140 MeV 3NFs bring theoretical predictions slightly away from data. The possibility of Coulomb force effects playing some role at this lowest energy prevents us from making a definite conclusion in this case. For the tensor analyzing powers the situation is totally different and these observables are challenging. The TM 3NF causes a drastic change with respect to the pure *NN* predictions; however, its effect leads to an even poorer agreement with the data. The TM′ and Urbana IX 3NFs generally give similar descriptions of the data. The effects of all 3NFs are angular dependent and become larger at higher energies. However, the experimental data are not explained by any of the 3NFs used. It is interesting to note that the theoretical predictions for these observables depend on the particular 3NF used and the effects of the TM′ and Urbana 3NFs are mostly opposite to the TM ones. Our results clearly indicate deficiencies in the spin-dependent part of present day 3NF models.

While one can probably neglect $pp$−Coulomb-force effects for the larger energies, it is very likely that relativity plays a role at our energies. Some indication of those effects comes from high-precision total $nd$ cross section data [27] and high-energy elastic scattering angular distributions [16]. Discrepancies between the data and nonrelativistic predictions become larger with increasing energy and cannot be removed by the 3NF effects (used up to now). A simple estimation of kinematical relativistic corrections already exhibits non-negligible effects. In order to get information on the magnitude of relativistic effects for spin observables a relativistic treatment such as proposed in Refs. [62,63] is required. Interference effects at medium angles for tensor analyzing powers make it probable that incorporation of relativity together with 3NFs might change the predictions for those spin observables.

We checked also the effects predicted by the phenomenological SO-3NF, which was introduced in order to solve the low-energy $A_y$ puzzle. This force acting on top of the AV18 and Urbana IX 3NF leads only to small effects at higher energies and it can be concluded that its effects are restricted mostly to the low-energy domain.

The approach in the framework of the coupled-channel formulation of $Nd$ elastic scattering [25,64] including the intermediate $\Delta$ gives complementary information on 3NF effects in the 3*N* continuum. The recent calculations based on the Paris potential [65] led to predictions that were in qualitative agreement with the effects of present day 3NF models. However, this model, based on the Paris potential, does not provide a good description of the *NN* data on the level of accuracy given by the modern *NN* potentials. Predictions that are fully converged with respect to the number of partial waves used and obtained with improved dynamics are required before quantitative conclusions on 3NF effects can be made in the framework of this approach.

The present status is only the very beginning of investigations to find the proper spin structure of the 3NF. The $Nd$ elastic cross section data seem to support the magnitude of the effects predicted by the present day forces. However, spin observables indicate that not every detail is under control. Further theoretical work is necessary in order to establish the proper spin structure of this term in the 3*N* potential energy. It should be guided by, e.g., the chiral effective field theory approach [66–68]. 3NF effects are especially large at higher energies and also a full relativistic treatment of the 3*N* continuum is called for.

At intermediate energies the present high-precision data are the first complete set of deuteron analyzing powers for $d$-$p$ elastic scattering covering a wide angular range and therefore serve as the best testing ground for investigation of 3NF effects. The most important constraints on the proper structure of 3NFs and the significance of relativity will come from a variety of high-precision data. The results of the present paper show that a measurement of tensor analyzing powers at even higher energies is very useful. Also at higher energies elastic scattering data for more complex spin observables such as some polarization transfer or spin correlation coefficients, which exhibit large 3NF dependent effects [17], would be helpful and should be measured. Another valuable source of information will be the $Nd$ breakup process with its rich spectrum of spin observables, for which at higher energies also large and 3*N* force-dependent effects have been predicted [69].

## ACKNOWLEDGMENTS

We acknowledge the outstanding work of the RIKEN Accelerator group for delivering excellent deuteron beams. We thank V. P. Ladygin for giving the opportunity for measuring the tensor analyzing power $A_{xz}$ data at 200 MeV during his beam time at the RIKEN Accelerator Research Facility. We also thank K. S. Itoh, T. Niizeki, T. Saito, N. Uchigashima, S. G. Reznikov, and A. Yu. Isupov for their help during the measurement. K.S. would like to acknowledge financial support of RIKEN. H.W. would like to thank the University of Tokyo for hospitality and support during his stay in Tokyo. This work was supported financially in part by Grant-in-Aid for Scientific Research Nos. 04402004 and 10304018 of the Ministry of Education, Science, Culture and Sports of Japan, by the Deutsche Forschungsgemeinschaft (H.K. and J.G.), and the Polish Committee for Scientific Research under Grant No. 2P03B02818. The numerical calculations were performed on the CRAY T90 and the CRAY T3E of the NIC in Jülich, Germany.

[1] R. B. Wiringa, V. G. J. Stoks, and R. Schiavilla, Phys. Rev. C **51**, 38 (1995).
[2] R. Machleidt, K. Holinde, and Ch. Elster, Phys. Rep. **149**, 1 (1987).
[3] R. Machleidt, Adv. Nucl. Phys. **19**, 189 (1989).
[4] R. Machleidt, Phys. Rev. C **63**, 024001 (2001).
[5] V. G. J. Stoks, R. A. M. Klomp, C. P. F. Terheggen, and J. J. de Swart, Phys. Rev. C **49**, 2950 (1994).
[6] A. Nogga, H. Kamada, and W. Glöckle, Phys. Rev. Lett. **85**, 944 (2000).

[7] J. Carlson and R. Schiavilla, Rev. Mod. Phys. **70**, 743 (1998).
[8] R. B. Wiringa, Steven C. Pieper, J. Carlson, and V. R. Pandharipande, Phys. Rev. C **62**, 014001 (2000).
[9] J. Fujita and H. Miyazawa, Prog. Theor. Phys. **17**, 360 (1957).
[10] S. A. Coon, M. D. Schadron, P. C. McNamee, B. R. Barrett, D. W. E. Blatt, and B. H. J. McKellar, Nucl. Phys. **A317**, 242 (1979); S. A. Coon and W. Glöckle, Phys. Rev. C **23**, 1790 (1981); S. A. Coon, Few-Body Syst., Suppl. **1**, 41 (1984); S. A. Coon and J. L. Friar, Phys. Rev. C **34**, 1060 (1996).
[11] S. A. Coon and M. T. Peña, Phys. Rev. C **48**, 2559 (1993).
[12] B. S. Pudliner, V. R. Pandharipande, J. Carlson, Steven C. Pieper, and R. B. Wiringa, Phys. Rev. C **56**, 1720 (1997).
[13] V. R. Pandharipande, Nucl. Phys. **A684**, 175 (2001).
[14] H. Witała, Th. Cornelius, and W. Glöckle, Few-Body Syst. **3**, 123 (1988).
[15] D. Hüber, H. Witała, and W. Glöckle, Few-Body Syst. **14**, 171 (1993).
[16] W. Glöckle, H. Witała, D. Hüber, H. Kamada, and J. Golak, Phys. Rep. **274**, 107 (1996).
[17] H. Witała, W. Glöckle, J. Golak, A. Nogga, H. Kamada, R. Skibiński, and J. Kuroś-Żołnierczuk, Phys. Rev. C **63**, 024007 (2001).
[18] A. Kievsky, M. Viviani, and S. Rosati, Phys. Rev. C **64**, 024002 (2001).
[19] H. Witała, D. Hüber, and W. Glöckle, Phys. Rev. C **49**, R14 (1994).
[20] Y. Koike and J. Haidenbauer, Nucl. Phys. **A463**, 365c (1987).
[21] W. Tornow and H. Witała, Nucl. Phys. **A637**, 280 (1998).
[22] J. L. Friar, D. Hüber, and U. van Kolck, Phys. Rev. C **59**, 53 (1999).
[23] D. Hüber, J. L. Friar, A. Nogga, H. Witała, and U. van Kolck, Few-Body Syst. **30**, 95 (2001).
[24] H. Witała, W. Glöckle, D. Hüber, J. Golak, and H. Kamada, Phys. Rev. Lett. **81**, 1183 (1998).
[25] S. Nemoto, K. Chmielewski, S. Oryu, and P. U. Sauer, Phys. Rev. C **58**, 2599 (1998).
[26] W. P. Abfalterer, F. B. Bateman, F. S. Dietrich, Ch. Elster, R. W. Finlay, W. Glöckle, J. Golak, R. C. Haight, D. Hüber, G. L. Morgan, and H. Witała, Phys. Rev. Lett. **81**, 57 (1998).
[27] H. Witała, H. Kamada, A. Nogga, W. Glöckle, Ch. Elster, and D. Hüber, Phys. Rev. C **59**, 3035 (1999).
[28] H. Shimizu, K. Imai, N. Tamura, K. Nisimura, K. Hatanaka, T. Saito, Y. Koike, and Y. Taniguchi, Nucl. Phys. **A382**, 242 (1982).
[29] S. P. Wells *et al.*, Nucl. Instrum. Methods Phys. Res. A **325**, 205 (1993).
[30] M. Poulet, A. Michalowicz, K. Kuroda, and D. Cronenberger, Nucl. Phys. **A99**, 442 (1967).
[31] H. Postma and R. Wilson, Phys. Rev. **121**, 1229 (1961).
[32] K. Kuroda, A. Michalowicz, and M. Poulet, Nucl. Phys. **88**, 33 (1966).
[33] R. E. Adelberger and C. N. Brown, Phys. Rev. D **5**, 2139 (1972).
[34] H. Rühl, B. Dechant, J. Krug, W. Lübcke, G. Spangardt, G. Spangardt, M. Steinke, M. Stephan, D. Kamke, J. Balewski, K. Bodek, L. Jarczyk, A. Stuzałakowski, W. Hajdak, St. Kistryn, R. Müller, J. Lang, R. Henneck, H. Witała, Th. Cornelius, and W. Glöckle, Nucl. Phys. **A524**, 377 (1991).
[35] R. Bieber, W. Glöckle, J. Golak, M. N. Harakeh, D. Hüber, H. Huisman, N. Kalantar-Nayestanaki, H. Kamada, J. G. Messchendorp, A. Nogga, H. Sakai, N. Sakamoto, M. Seip, M. Volkerts, S. Y. van der Werf, and H. Witała, Phys. Rev. Lett. **84**, 606 (2000).
[36] E. J. Stephenson, H. Witała, W. Glöckle, H. Kamada, and A. Nogga, Phys. Rev. C **60**, 061001(R) (1999).
[37] R. V. Cadman, J. Brack, W. J. Cummings, J. A. Fedchak, B. D. Fox, H. Gao, W. Glöckle, J. Golak, C. Grosshauser, R. J. Holt, C. E. Jones, H. Kamada, E. R. Kinney, M. A. Miller, W. Nagengast, A. Nogga, B. R. Owen, K. Rith, F. Schmidt, E. C. Schulte, J. Sowinski, F. Sperisen, E. L. Thorsland, R. Tobey, J. Wilbert, and H. Witała, Phys. Rev. Lett. **86**, 967 (2001).
[38] K. Ermisch *et al.*, Phys. Rev. Lett. **86**, 5862 (2001).
[39] H. Witała, W. Glöckle, L. E. Antonuk, J. Arvieux, D. Bachelier, B. Bonin, A. Boudard, J. M. Cameron, H. W. Fielding, M. Garçon, F. Jourdan, C. Lapointe, W. J. McDonald, J. Pasos, G. Roy, I. The, J. Tinslay, W. Tornow, J. Yonnet, and W. Ziegler, Few-Body Syst. **15**, 67 (1993).
[40] J. Arvieux, S. D. Baker, R. Beurtey, M. Boivin, J. M. Cameron, D. A. Hutcheon, J. Banaigs, J. Berger, A. Codino, J. Duflo, L. Goldzahl, F. Plouin, A. Boudard, G. Gaillard, Nguyen Van Sen, and Ch. Perdrisat, Phys. Rev. Lett. **50**, 19 (1983).
[41] M. Garçon *et al.*, Nucl. Phys. **A458**, 287 (1986).
[42] H. Sakai, K. Sekiguchi, H. Witała, W. Glöckle, M. Hatano, H. Kamada, H. Kato, Y. Maeda, A. Nogga, T. Ohnishi, H. Okamura, N. Sakamoto, S. Sakoda, Y. Satou, K. Suda, A. Tamii, T. Uesaka, T. Wakasa, and K. Yako, Phys. Rev. Lett. **84**, 5288 (2000).
[43] H. Okamura *et al.*, in *Polarized Ion Sources and Polarized Gas Targets*, edited by L. W. Andersen and Willy Haeberli, AIP Conf. Proc. No. 293 (AIP, New York, 1994), p. 84.
[44] H. Okamura *et al.*, in *High Energy Spin Physics*, edited by Kenneth J. Heller and Sandra L. Smith, AIP Conf. Proc. No. 343 (AIP, Woodbury, New York, 1995), p. 123.
[45] T. Ichihara *et al.*, Nucl. Phys. **A569**, 287c (1994).
[46] N. Sakamoto, H. Okamura, T. Uesaka, S. Ishida, H. Otsu, T. Wakasa, Y. Satou, T. Niizeki, K. Katoh, T. Yamashita, K. Hatanaka, Y. Koike, and H. Sakai, Phys. Lett. B **367**, 60 (1996).
[47] H. Okamura, S. Fujita, Y. Hara, K. Hatanaka, T. Ichihara, S. Ishida, K. Katoh, T. Niizeki, H. Ohnuma, H. Otsu, H. Sakai, N. Sakamoto, Y. Satou, T. Uesaka, T. Wakasa, and T. Yamashita, Phys. Lett. B **345**, 1 (1995).
[48] T. Ohnishi, H. Sakai, H. Okamura, S. Ishida, H. Otsu, N. Sakamoto, T. Uesaka, T. Wakasa, Y. Satou, S. Fujita, T. Nonaka, and E. J. Stephenson, Phys. Lett. B **438**, 27 (1998); **458**, 564(E) (1999).
[49] T. Uesaka, H. Sakai, H. Okamura, T. Ohnishi, Y. Satou, S. Ishida, N. Sakamoto, H. Otsu, T. Wakasa, K. Itoh, K. Sekiguchi, and T. Wakui, Phys. Lett. B **467**, 199 (1999).
[50] H. Kamada, D. Hüber, and A. Nogga, Few-Body Syst. **30**, 121 (2001).
[51] T. Uesaka *et al.*, RIKEN Accel. Prog. Rep. **33**, 153 (2000).
[52] R. A. Arndt and L. D. Roper, Scattering Analysis Program (SAID), Virginia Polytechnic Institute and State University (unpublished); see also Phys. Rev. C **56**, 3005 (1997), and references therein.
[53] G. G. Ohlsen, Rep. Prog. Phys. **35**, 717 (1972).
[54] D. Hüber, H. Kamada, H. Witała, and W. Glöckle, Acta Phys. Pol. B **28**, 1677 (1997).

[55] A. Nogga, D. Hüber, H. Kamada, and W. Glöckle, Phys. Lett. B **409**, 19 (1997).
[56] S. A. Coon, M. T. Peña, and D. O. Riska, Phys. Rev. C **52**, 2925 (1995).
[57] H. Witała, D. Hüber, W. Glöckle, J. Golak, A. Stadler, and J. Adam, Jr., Phys. Rev. C **52**, 1254 (1995).
[58] A. Kievsky, M. Viviani, and S. Rosati, Phys. Rev. C **52**, R15 (1995).
[59] A. Kievsky, S. Rosati, W. Tornow, and M. Viviani, Nucl. Phys. **A607**, 402 (1996).
[60] A. Kievsky, Phys. Rev. C **60**, 034001 (1999).
[61] H. Kamada *et al.* (unpublished).
[62] H. Kamada and W. Glöckle, Phys. Rev. Lett. **80**, 2547 (1998).
[63] H. Kamada, Few-Body Syst., Suppl. **12**, 433 (2000).
[64] P. U. Sauer, K. Chmielewski, S. Nemoto, and S. Oryu, Nucl. Phys. **A684**, 531 (2001).
[65] M. Lacombe, B. Loiseau, J. M. Richard, R. Vinh Mau, J. Coté, P. Pirès, and R. de Tourreil, Phys. Rev. C **21**, 861 (1980).
[66] U. van Kolck, Phys. Rev. C **49**, 2932 (1994).
[67] E. Epelbaum, W. Glöckle, and U.-G. Meißner, Nucl. Phys. **A637**, 107 (1998).
[68] E. Epelbaum, W. Glöckle, and U.-G. Meißner, Nucl. Phys. **A671**, 295 (2000).
[69] H. Witała, W. Glöckle, H. Kamada, A. Nogga, J. Golak, J. Kuroś-Żołnierczuk, and R. Skibiński, in *Spin 2000*, edited by Hiroyasu Ejiri, Kichiji Hatanaka, Kenichi Imai, and Takashi Nakano, AIP Conf. Proc. No. 570 (AIP, Melville, NY, 2001), p. 208.